Chemical Engineering Science 66 (2011) 3204–3211

Contents lists available at ScienceDirect

Chemical Engineering Science

journal homepage: www.elsevier.com/locate/ces

On the drag force of bubbles in bubble swarms at intermediate and high Reynolds numbers

I. Roghair *, Y.M. Lau, N.G. Deen, H.M. Slagter, M.W. Baltussen, M. Van Sint Annaland, J.A.M. Kuipers

Multiphase Reactors Group, Department of Chemical Engineering and Chemistry, Eindhoven University of Technology, P.O. Box 513, 5612 AZ Eindhoven, The Netherlands

ARTICLE INFO

Article history:
Received 15 October 2010
Received in revised form
10 February 2011
Accepted 10 February 2011
Available online 19 February 2011

Keywords:
Numerical modeling
Front tracking
Bubbly flows
Bubble swarms
Drag force
Closure relation

ABSTRACT

An accurate and fast simulation of large-scale gas/liquid contact apparatusses, such as bubble columns, is essential for the optimization and further development of many (bio)chemical and metallurgical processes. Since it is not feasible to simulate an entire industrial-scale bubble column in full detail from first principles (direct numerical simulations), higher-level models rely on algebraic closure relations to account for the most important physical phenomena prevailing at the smallest length and time scales, while keeping computational demands low. The most important closure for describing rising bubbles in a liquid is the closure for the drag force, since it dominates the terminal rise velocity of the bubbles.

Due to the very high gas loadings used in many industrial processes, bubble–bubble (or 'swarm') interactions need to be accounted for in the drag closure. An advanced front-tracking model was employed, which can simulate bubble swarms up to 50% gas hold-up without the problem of (numerical) coalescence. The influence of the gas hold-up for mono-disperse bubble swarms with different bubble diameters (i.e. Eötvös numbers) was quantified in a single drag correlation valid for the intermediate to high Reynolds numbers regime ($1 \leq$ Eo ≤ 5). Also the physical properties of the liquid phase were varied, but the simulation results revealed that the drag force coefficient was independent of the Morton number. The newly developed correlation has been implemented in a larger-scale model, and the effect of the new drag closure on the hydrodynamics in a bubble column is investigated in a separate paper (Lau et al., this issue).

1. Introduction

1.1. Bubbly flows in industrial practice

Bubbly flows are dispersed two-phase flows involving a gas and a liquid phase, which are brought into contact with each other in such a way that the gas forms bubbles which rise through the liquid. Bubbly flows are often encountered in industrial environments, for instance in bubble columns in the (bio-)chemical or metallurgical industry. In chemical processes, (reacting) components are exchanged between a multitude of bubbles ('bubble swarms') and the continuous liquid phase, while in metallurgical applications the (argon) bubbles are mainly used to induce a mixing current in a ladle of molten steel.

In either case, the gas hold-up (or gas fraction) is an important parameter to control the efficiency and hydrodynamics in a bubble column. At high gas fractions, many bubbles are injected simultaneously, forming bubble swarms which adopt a behavior very different from single, undisturbed rising bubbles. Numerical studies on bubbly flows at industrial scales need to be performed to investigate the effect of the gas fraction on the process efficiency, however, this cannot be done accurately without detailed knowledge on the physics occurring at small scales. Therefore, this paper focuses on the drag force acting on bubbles rising in a swarm which is compared to the drag force on single rising bubbles in an infinite, initially quiescent liquid.

1.2. Objectives and outline

The objective of this work is to develop a closure correlation for the drag force acting on a bubble in a mono-disperse swarm accounting for the presence of neighboring bubbles, referred to as the swarm effect, in particular as a function of the gas hold-up using direct numerical simulations. In addition, the effect of bubble size and physical properties is taken into account. The physical properties used vary from air bubbles in water (which is most significant for industrial applications) to more viscous liquids. The closure effectively provides larger-scale models with accurate information on the momentum interchange between the two phases, and in a separate paper the effect of the new drag closure on the hydrodynamics in a bubble column has been investigated (Lau et al., this issue).

The outline of this paper is as follows: we will first discuss our multi-scale modeling approach and summarize work that has

* Corresponding author. Tel.: +31 40 247 3975; fax: +31 40 247 5833.
E-mail address: i.roghair@tue.nl (I. Roghair).

0009-2509/$ - see front matter © 2011 Elsevier Ltd. All rights reserved.
doi:10.1016/j.ces.2011.02.030

been done on single rising bubbles and swarms of bubbles. Subsequently, we will outline the importance of the drag force in bubbly flows and the correction factor for the drag coefficient in bubble swarms. Then, the main characteristics and computational setup of the used front-tracking model and simulations for mono-disperse bubble swarms will be summarized. Finally, a closure for the drag coefficient is derived from the simulation results, that fully accounts for the bubble size and presence of neighboring bubbles.

2. Drag in bubbly flows

2.1. Multi-scale modeling

Bubble columns are commonly operated at very large scales, in the order of tens of meters. At such scales it is computationally impossible to resolve the flow of the fluids in full detail. Therefore, we have adopted the multi-scale modeling technique (Deen et al., 2004; van Sint Annaland et al., 2003), where large-scale models are provided with accurate, yet easy to compute, closure correlations derived from more-detailed smaller-scale models. Together, the models form a hierarchy (see Fig. 1). At the smallest scale (typically in the order of centimeters), closures are derived using direct numerical simulations (DNS, of which a variety of modeling techniques are available (see Van Sint Annaland et al., 2006)). In DNS, no assumptions are required and the gas/liquid behavior follows immediately from solving the Navier–Stokes equations.

The simulation of intermediate scales (in the order of meters) is done using the discrete bubble model (DBM). In the DBM, the bubbles are represented by Lagrangian spheres, while the liquid flow field is calculated with the Navier–Stokes equations. The bubble dynamics are not fully resolved, but rather determined using closure correlations, hereby saving huge amounts of computation time.

Even larger than the DBM model, the two-fluid model (TFM) is an Euler–Euler method that simulates the two-phase flow at industrial scales, i.e. tens of meters, using a phase fraction parameter. This work, however, focuses on the derivation of a closure for the drag coefficient using DNS, for further use in the DBM and other higher-level models, and in a related paper we will investigate the effect of the new closure on the bubble column hydrodynamics at large scales.

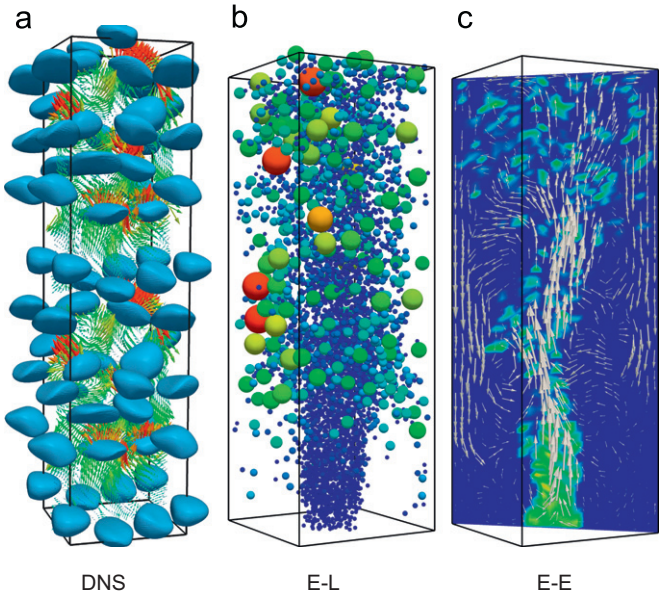

Fig. 1. Gas–liquid multi-scale modeling hierarchy with left: direct numerical simulations, center: Euler–Lagrangian method and right: Euler–Euler method. The models displayed are in-house developed and visualized using ParaView.

2.2. Buoyant bubble characteristics

The work that has been carried out on single rising bubbles in an initially quiescent liquid has tremendously increased our fundamental understanding of the physics of buoyant rising bubbles. Clift et al. (1978) already indicated that the bubble rise velocity (which is directly correlated to the drag coefficient) and the bubble shape is dictated by an interplay of various dimensionless numbers; the Eötvös number Eo, the Reynolds number Re and Morton number Mo (Eqs. (1)–(3)), defined as follows:

$$\mathrm{Eo} = \frac{g(\rho_l - \rho_g)d_b^2}{\sigma} \tag{1}$$

$$\mathrm{Re} = \frac{\rho_l v_{b,z} d_b}{\mu_l} \tag{2}$$

$$\mathrm{Mo} = \frac{g\mu_l^4(\rho_l - \rho_g)}{\rho_l^2 \sigma^3} \tag{3}$$

The Eötvös number represents the ratio between buoyancy and surface tension forces and is together with the Reynolds number (ratio between inertial and viscous forces) a good indicator of the bubble shape. The Morton number is the ratio of viscous and surface tension forces, taking the physical properties of gas and liquid into account. The importance of these numbers is reflected by their use in drag correlations for single rising bubbles derived by different groups (e.g. Tomiyama, 1998; Dijkhuizen et al., 2010a). These correlations also indicate that different regimes can be distinguished; the drag on spherical and ellipsoidal bubbles is mainly determined by the viscous drag (low Reynolds and Eötvös numbers), in contrast to larger bubbles, which are wobbling or spherical capped bubbles (higher Reynolds and Eötvös numbers).

In addition, the air bubbles in water regime with a very low Morton number ($\mathrm{Mo} = 2.5 \times 10^{-11}$) are notoriously difficult and often causes numerical problems, which is why most results can be found for the low-Reynolds/low-Eötvös regime (i.e. spherical and ellipsoidal bubbles). However, in many industrial applications the higher Reynolds and Eötvös regimes are more important. This work employs a front-tracking model, with which multiple air bubbles in water (3–6 mm diameter bubbles) have been simulated with Eötvös numbers between 1 and 5 and Reynolds numbers ranging from 150 up to 1200 (i.e. wobbling regime).

2.3. Determination of the drag coefficient

The DBM uses a macroscopic force balance, to calculate the velocity for each individual bubble. The force balance is given in Eq. (4), respectively, accounting for the forces of gravity, pressure gradient, drag, lift, virtual mass and wall forces, see Darmana et al. (2009):

$$m\frac{d\overline{v}}{dt} = \overline{F}_G + \overline{F}_P + \overline{F}_D + \overline{F}_L + \overline{F}_{VM} + \overline{F}_W \tag{4}$$

For the latter four terms on the right-hand side, the DBM requires closure correlations, which can be found throughout literature. See for instance Tomiyama (1998), Magnaudet and Eames (2000), Tomiyama et al. (2002), Dijkhuizen et al. (2005, 2010a,c) to name just a few. From these forces, the drag force is unmistakably the most important force in determining the bubble rise

velocity (and hence an important factor in the efficiency of the entire process), usually implemented using Eq. (5), where C_D is the drag coefficient:

$$\overline{F}_D = -\tfrac{1}{8} C_D \rho_l \pi d_b^2 |\overline{v}-\overline{u}|(\overline{v}-\overline{u}) \tag{5}$$

When the macroscopic force balance on a bubble is considered at (pseudo) steady state, the time-averaged drag force exactly balances the buoyancy force, which is a combination of the force of gravity and the hydrostatic pressure. Hence, the steady-state force balance on a single buoyant rising bubble is given by

$$\begin{aligned}\langle \overline{F}_D \rangle &= \langle \overline{F}_P \rangle + \langle \overline{F}_G \rangle = -V_b \nabla p + \rho_g V_b \overline{g} \\ &= -V_b \rho_l \overline{g} + V_b \rho_g \overline{g}\end{aligned} \tag{6}$$

using the brackets to indicate time-averaging. The (time-averaged) drag coefficient $C_{D,\infty}$ can now be obtained by combining Eqs. (5) and (6) resulting in Eq. (7), in which the time-averaged bubble slip velocity needs to be acquired from the simulations. In addition, note that for single bubbles rising in an infinite, initially quiescent liquid, the liquid velocity $\overline{u}$ will be zero, and the (time-averaged) bubble rise velocity v_∞ remains

$$C_{D,\infty} = \frac{4}{3}\frac{d_b(\rho_l-\rho_g)\overline{g}}{\rho_l|\overline{v}-\overline{u}|^2} = \frac{4}{3}\frac{d_b(\rho_l-\rho_g)\overline{g}}{\rho_l|\overline{v}_\infty|^2} \tag{7}$$

For bubble swarms, the approach is slightly different. Analogous to Simonnet et al. (2007), Eq. (7) should be modified to account for the local gas hold-up. Indeed, the buoyancy force acting on a bubble in a swarm depends on the density difference between the gas phase and the gas/liquid suspension, which reduces the pressure force exerted on a bubble in a swarm in comparison to the force exerted on a single bubble in a liquid. The time-averaged drag force on a bubble in a swarm reads

$$\begin{aligned}\langle \overline{F}_D \rangle &= \langle \overline{F}_P \rangle + \langle \overline{F}_G \rangle = -V_b \nabla p + \rho_g V_b \overline{g} \\ &= -V_b((1-\alpha)\rho_l - \alpha\rho_g)\overline{g} + V_b \rho_g \overline{g} \\ &= (1-\alpha)(\rho_g-\rho_l)\overline{g} V_b\end{aligned} \tag{8}$$

Therefore, in the case of bubble swarms, a correction factor has to be taken into account if the drag coefficient is defined via Eq. (5):

$$\frac{C_D}{(1-\alpha)} = \frac{4}{3}\frac{d_b(\rho_l-\rho_g)\overline{g}}{\rho_l|\overline{v}-\overline{u}|^2} \tag{9}$$

Combining Eqs. (7) and (9) shows that the relative drag coefficient is directly related to the relative velocity of a bubble:

$$\frac{C_D}{C_{D,\infty}(1-\alpha)} = \left(\frac{v_\infty}{|\overline{v}-\overline{u}|}\right)^2 \tag{10}$$

It is important to note that, when calculating the drag coefficient for a bubble rising in a swarm, the assumption of a steady-state or time-averaged balance between drag and buoyancy forces implies that either the time-averaged effect of other forces (viz. lift and virtual mass due to local velocity gradients and bubble acceleration and deceleration) is negligible or, alternatively, assumed to be lumped into the time-averaged drag coefficient.

Another issue that has to be addressed is the liquid velocity $\overline{u}$, which is very important in the calculation of the drag coefficient since it depends on the slip velocity. The liquid velocity used in this work is the liquid velocity of the entire domain. Since the gas phase moves upward and the total momentum in the domain is kept at zero by subtracting the domain fluid velocity, a net downflow of the liquid is obtained. The liquid velocity can be easily calculated from the phase fraction in the Eulerian cells using the following equation:

$$\overline{u} = \frac{1}{n_{\text{cells}}}\sum_{n=1}^{n_{\text{cells}}} \phi_n \overline{w}_n \tag{11}$$

where ϕ_n is the liquid fraction in cell n and $\overline{w}_n$ is the fluid flow velocity of cell n.

2.4. Single rising bubbles

The drag coefficient of bubbles in a swarm will be presented relative to the drag coefficient on a single rising bubble in an infinite, initially quiescent liquid. In this work, we will use the correlation for the drag coefficient for a single bubble derived by Dijkhuizen et al. (2010a):

$$C_{D,\infty} = \sqrt{C_D(\text{Re})^2 + C_D(\text{Eo})^2} \tag{12}$$

with (see also Mei et al., 1994):

$$C_D(\text{Re}) = \frac{16}{\text{Re}}\left(1 + \frac{2}{1+\frac{16}{\text{Re}}+\frac{3.315}{\sqrt{\text{Re}}}}\right) \tag{13}$$

$$C_D(\text{Eo}) = \frac{4\text{Eo}}{\text{Eo}+9.5} \tag{14}$$

2.5. Bubble swarms

A number of correlations for the drag coefficient on dispersed elements in two-phase flow can be found in literature. Sometimes the correlation describes the drag coefficient, and sometimes the steady-state bubble rise velocity but these are directly correlated, as was shown in the previous sections. Most of the work found in literature is derived from experiments.

We adopt the approach of Rusche and Issa (2000), by defining a correction function $f(\alpha,\ldots)$ accounting for the local gas hold-up (and possibly other factors) with respect to the single rising bubble drag coefficient:

$$\frac{C_{D,\text{swarm}}}{C_{D,\infty}(1-\alpha)} = f(\alpha,\ldots) \tag{15}$$

The correction function proposed by Rusche and Issa (2000) for bubbly flows was derived from a fit of numerous experimental data found in literature (note that the factor $(1-\alpha)$ is included in the correction factor):

$$f(\alpha) = [\exp(3.64\alpha) + \alpha^{0.864}] \tag{16}$$

Simonnet et al. (2007) give a short overview of correlations, describing the rise velocity of bubbles in a swarm in a form that was pioneered by Richardson and Zaki (1954). To acknowledge them, the exponent n was termed the Richardson and Zaki exponent:

$$f(\alpha) = (1-\alpha_{\text{glob}})^{-2n} \tag{17}$$

Bridge et al. (1964) proposed an exponent of $n = 1.39$, which was later modified to Eq. (18) by Lockett and Kirkpatrick (1975) to account for shape deformations:

$$f(\alpha) = [(1-\alpha_{\text{glob}})^{1.39} \times (1+2.55\alpha_{\text{glob}}^3)]^{-2} \tag{18}$$

Note that Eqs. (17) and (18) were rewritten as relative drag coefficients using Eq. (10). Simonnet et al. (2007) derived a drag closure on experiments using laser Doppler velocimetry (for the liquid velocity) and a double optical probe (for the bubble properties), up to a gas fraction of 35%:

$$f(\alpha) = [(1-\alpha_{\text{loc}})^m + (4.8\alpha_{\text{loc}}/(1-\alpha_{\text{loc}}))^m]^{-2/m} \tag{19}$$

They define a critical value for the gas hold-up (which they find at 15%), where the transition between hindered and cooperative rise occurs, setting $m = 25$. A discussion of the implementation of their drag closure in an Euler–Euler and an Euler–Lagrangian

model can be found in Simonnet et al. (2008). A different experimental approach, that does not perturb the flow, relies on optical methods. However, these methods are appropriate either for (very) low gas fractions in three-dimensional setups (see e.g. Martínez Mercado et al., 2010 using particle tracking velocimetry), or by pseudo-two-dimensional columns making use of digital image analysis (Acuña and Finch, 2010). In three-dimensional columns at high gas fractions, the bubbles obstruct visual access. For dense, three-dimensional swarms, numerical simulations provide a good way to non-invasively measure a bubble swarm, which will be discussed in the next section.

3. DNS modeling

3.1. Model types

Front-tracking modeling is a well-known direct numerical simulations (DNS) method (a.o. Unverdi and Tryggvason, 1992; Van Sint Annaland et al., 2006; Dijkhuizen et al., 2010b) to simulate multiphase flows with deformable interfaces in full detail. The main advantage of using a front-tracking model is that bubbles do not coalesce unless a specific merge condition is implemented (see for instance Singh and Shyy, 2007).

Other DNS methods employed to simulate bubble swarms are the level-set method (see Smolianski et al., 2008 for two-dimensional simulations of a structured array of ellipsoidal and spherical bubbles) or volume of fluid (VoF) methods, but these methods tend to merge bubbles automatically (and unphysically), unless a special prevention algorithm is implemented. Another popular technique to simulate bubbly flows is the lattice-Boltzmann method (LBM). Since LBM is highly parallellizable, it is in theory capable of simulating large bubbly flows. However, the notoriously difficult air–water regime causes numerical difficulties (Sankaranarayanan et al., 2002) and to the authors' knowledge, no work using LBM has appeared yet discussing the rise of bubble swarms in this regime.

Table 1
Physical properties for the air–water (base case) simulations.

Property	Symbol	Value
Gas density	ρ_g	1.25 kg/m^3
Gas viscosity	μ_g	1.8×10^{-5} Pa s
Liquid density	ρ_l	1000 kg/m^3
Liquid viscosity	μ_l	10^{-3} Pa s
Surface tension coefficient	σ	0.073 N/m

3.2. Front-tracking model

A short introduction of the front-tracking method employed for this work is given here. For a more-detailed description, see Dijkhuizen et al. (2010b).

The fluid flow is described with a single fluid formulation of the Navier–Stokes equation, while mass conservation is enforced by the continuity equation:

$$\rho\frac{\partial\overline{u}}{\partial t} = -\nabla p - \rho\nabla\cdot(\overline{u}\overline{u}) + \nabla\cdot\boldsymbol{\tau} + \rho\overline{g} + \overline{F_\sigma} \tag{20}$$

$$\nabla\cdot\overline{u} = 0 \tag{21}$$

where $\overline{u}$ is the fluid velocity, $\boldsymbol{\tau}$ is the stress tensor and p is the pressure. We use a finite difference technique to discretize the velocity components on a staggered grid while the scalar values such as the pressure are located in the Eulerian cell centers. Solving the flow field and pressure quantities is done using a two-stage projection-correction method. The stress tensor is discretized semi-implicitly, and therefore the three velocity components u_x, u_y and u_z are solved separately (projection). Then, the mass balance is enforced via a pressure correction step. Both steps use an ICCG matrix solver. The computational domain is bounded by full three-dimensional periodic conditions, so that an infinite swarm of bubbles is mimicked. The interfaces between the phases are tracked using Lagrangian control points. The interconnection between these points form a mesh of triangular markers. In Eq. (20), $\overline{F}_\sigma$ accounts for the surface tension force, that can be directly calculated from the positions of markers on the interface on a sub-grid scale.

After the fluid flow has been calculated, the Lagrangian control points are moved to their new locations at every time step. The fluid flow is interpolated using cubic splines, which are constructed from the region around each bubble separately. The presence of other bubbles within this region, does not affect the construction of the splines, because the flow field is continuous over the interface. The markers are advected with the interpolated fluid flow using 4th order Runge–Kutta time stepping. From the marker points, the centroid of the bubbles can be calculated and hence, the position, velocity and shape of the rising bubbles are stored each time step. The phase fraction is derived from the marker position analytically; from the marker center positions, the volume of the bubble phase above each marker can be calculated for each Eulerian grid cell. The density of each Eulerian cell is calculated by weighted averaging with the phase fraction. The viscosity is obtained by harmonic averaging of the kinematic viscosities, also weighted by the phase fraction (Prosperetti, 2002).

3.3. Simulation settings

Initially, the bubbles are placed randomly throughout the periodic domain. The physical properties of the gas and liquid phases are, for the base case, setup using the values for air bubbles in water

Table 2
Physical properties for the simulations with different Morton and Eötvös numbers.

Case	d_b (mm)	μ_l (Pa s)	ρ_l (kg/m^3)	σ N m	$-\log$ (Mo)	Eo	Comment
1	3.0	1.0×10^{-3}	1000	0.073	10.6	1.21	Air–water
2	6.0	1.5×10^{-3}	750	0.138	10.6	1.92	
3	4.0	1.0×10^{-3}	1000	0.073	10.6	2.15	Air–water
4	6.0	2.0×10^{-3}	1250	0.171	10.6	2.58	
5	6.0	1.0×10^{-3}	1000	0.073	10.6	4.83	Air–water
6	4.5	1.5×10^{-3}	950	0.073	9.87	2.58	
7	4.5	2.0×10^{-3}	1025	0.042	8.67	4.83	
8	4.5	1.0×10^{-3}	840	0.138	11.35	1.21	
9	1.0–7.0	1.0×10^{-1}	1000	0.073	2.6	0.13–6.6	Cubic array

(see Table 1). These properties were changed to investigate the influence of the Eötvös and Morton number. The properties that were changed and the resulting Morton and Eötvös numbers are shown in Table 2. For each case, multiple simulations were performed at different gas fractions, which vary between 5% and 45%. The cases 1–5 are meant to study the influence of the Eötvös number, whilst keeping the Morton number constant. Cases 6–8 are used to study the influence of the Morton number, so we have chosen a set of three Eötvös numbers to which we should compare the results of these cases. Case 9 was used only for cubic arrays of bubbles. For the cases described, the bubble Reynolds number is typically between 150 and 1200.

Although it depends on the exact conditions (viscosity of the liquid phase, bubble diameter, gas fraction), the simulation time is typically about 1 s, using a time step of 1×10^{-5} s. From Eq. (9), we have seen that we only require the bubble slip velocity resulting from the simulation to calculate the drag coefficient. Of course, the slip velocity oscillates largely, because of the wobbling regime and bubble–bubble interactions. Therefore, the time-averaged slip velocity is used excluding the first 0.2 s leaving out start-up effects which are, obviously, much less seen at higher gas fractions because of the increased number of bubble–bubble interactions. Using case 3, we have determined that the time average of a time interval of only 0.2 s is already sufficient to yield a time-averaged slip velocity that deviates less than 2% from the time-averaged value using the entire time interval (0.2–1.0 m/s). Thus, for the cases with high gas fractions we can be confident that enough datapoints have been acquired, however, for low Reynolds numbers (i.e. more viscous liquids) the averaging period may need to be longer.

3.4. Grid size

The required Eulerian (equidistant and uniform) grid size was already investigated for single rising bubbles by Dijkhuizen et al. (2010a). It was found that when using no less than 20 grid cells on a bubble diameter, the results show no significant influence of the grid size. A similar analysis on bubble swarms has been performed, showing that using at least 15 grid cells on a bubble diameter no effect of the grid size on the rise velocity was observed, and for the actual simulations 20 grid cells have been used.

The length of the edges of the triangular markers, which make up the interface of the bubbles, has been specified to be minimally 0.2, and maximally 0.5 times the edge length of an Eulerian grid cell. Simulations with smaller triangle edges did not result in better resolved interface dynamics, but larger triangle edges made the shape oscillations more stiff.

4. Number of bubbles

4.1. Cubic array

Sankaranarayanan et al. (2002) have derived a drag correction for the gas fraction, using the LBM method and a single bubble in a periodic domain for gas fractions up to 20%. They observed cooperative rise, which was explained by the wake of the bubble that eventually stretches through the entire domain to affect the next bubble (periodic image). They discussed the deformation toward a more spherical shape (or even become prolate) for increasing gas fractions, due to less suction at the sides of the bubble as compared to a single rising bubble.

We have first performed simulations using case 9 (Table 2), a single bubble in the center of a periodic domain to mimick a cubic array of bubbles, and normalized them with the drag coefficient of a single rising bubble $C_{D,\infty}$ (see Fig. 2 and related work

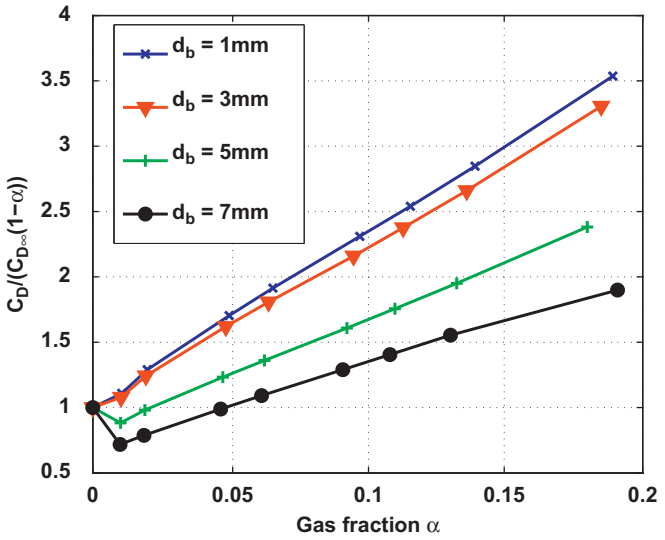

Fig. 2. Drag on a single bubble in the center of a periodic domain for different bubble diameters.

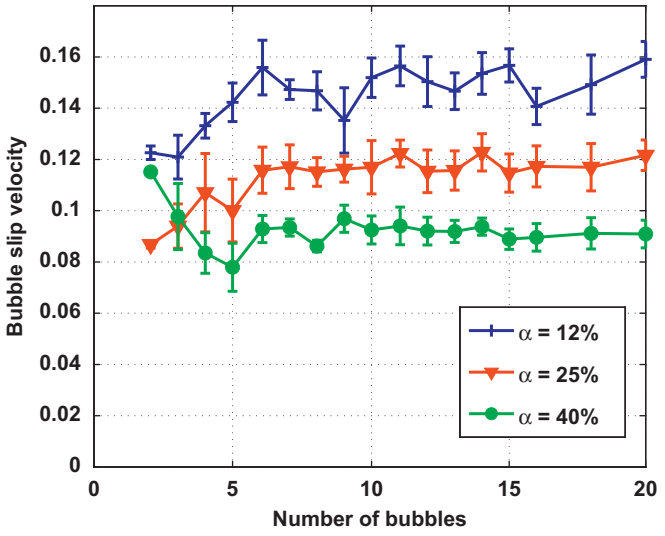

Fig. 3. Computed time-averaged, number averaged slip velocity as a function of the number of bubbles in the periodic domain for three different gas hold-ups. The errorbars show the standard deviation in the fluctuations of the slip velocity.

of Dijkhuizen, 2008; Dijkhuizen et al., 2008). At very low gas hold-ups and large bubbles, cooperative rise is observed, probably due to the wake of the leading bubble (periodic image). At higher gas fractions, this effect is not seen, which was attributed to the weaker liquid flow downward between the bubble and its (periodic) neighbors on the sides, since they are too close to each other. Interestingly, the normalized drag coefficient increases linearly with the gas fraction. The slope is highest for the smallest bubbles, since they cannot deform and adapt their shape to reduce the drag.

4.2. Required minimum number of bubbles

Of course a cubic array of bubbles does not capture all the dynamics, since bubbles cannot overtake or move away from each other. The number of bubbles used in a periodic domain, that truthfully represents a bubble swarm thus has to be determined. Bunner and Tryggvason (2002) already mentioned that

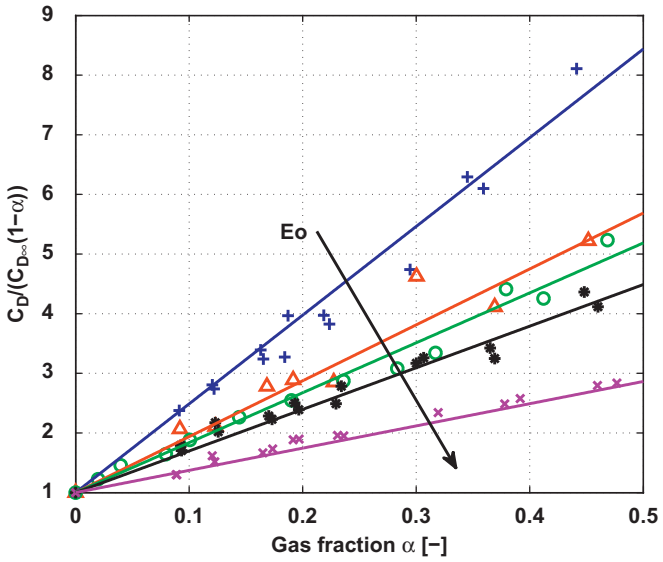

Fig. 4. The drag coefficient of a bubble in a swarm, normalized with the drag on a single rising bubbles as a function of the gas fraction, for series of different Eötvös numbers. Legend: +, Eo = 1.21; △, Eo = 1.92; ◦, Eo = 2.15; ∗, Eo = 2.58; ×, Eo = 4.83.

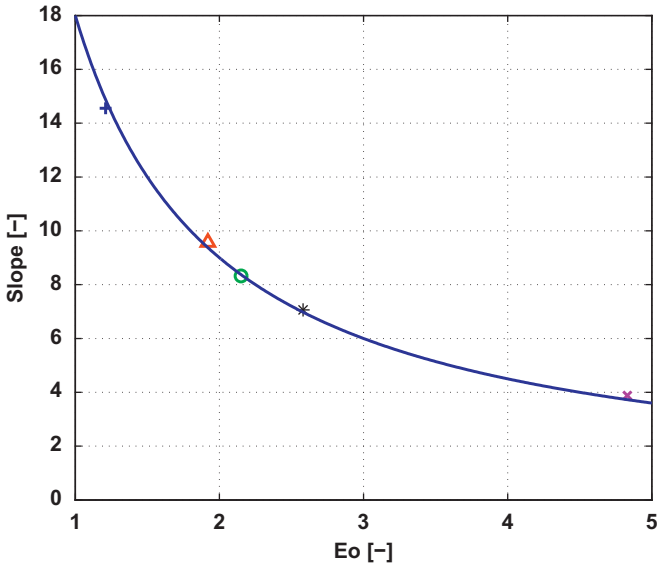

Fig. 5. The function g as a function of the Eötvös number (symbols are identical to Fig. 4; the line is the fit given by Eq. (23)).

the minimum number of bubbles is about 12, for their own (peculiar) set of physical properties. Using air bubbles in water (see Table 1), the number of bubbles has been varied for three different gas fractions (12%, 25% and 40%) between 1 and 20 (see Fig. 3). It was determined that at least eight bubbles should be used for the cases with 25% and 40% gas hold-up, and at least 10 bubbles for the 12% gas hold-up case. The variation of rise velocities that are seen using more than 10 bubbles are within the error margins. A clear distinction between the velocities at different gas hold-ups is observed already from five bubbles or more.

5. Drag correlation

5.1. Eötvös dependency

The relative drag coefficient resulting from the simulations was sorted into series with identical Eötvös numbers. Plotting the relative drag coefficients against the gas fraction showed a linear relation with the gas fraction, which starts at $C_D/C_{D,\infty}=1$ for single rising bubbles, i.e. $\alpha=0$. The slope of the linear relation varies significantly with the Eötvös number, as shown in Fig. 4. Hence the correlation, including a correction factor for the pressure gradient, is now written as Eq. (22), where the function g incorporating Eo determines the slope of the drag coefficient vs. α:

$$\frac{C_D}{C_{D,\infty}(1-\alpha)} = f(\alpha) = 1 + g(\mathrm{Eo})\alpha \tag{22}$$

A least squares fit has yielded:

$$\frac{C_D}{C_{D,\infty}(1-\alpha)} = 1 + \left(\frac{18}{\mathrm{Eo}}\right)\alpha \tag{23}$$

Fig. 5 shows that the proposed function for g(Eo) well describes the simulation results.

5.2. Correlation performance and comparison

In the range of $1 \le \mathrm{Eo} \le 5$ the correlation performs particularly well, describing the drag coefficient found in the simulations within, on average, 1.5% accuracy, while the maximum deviation

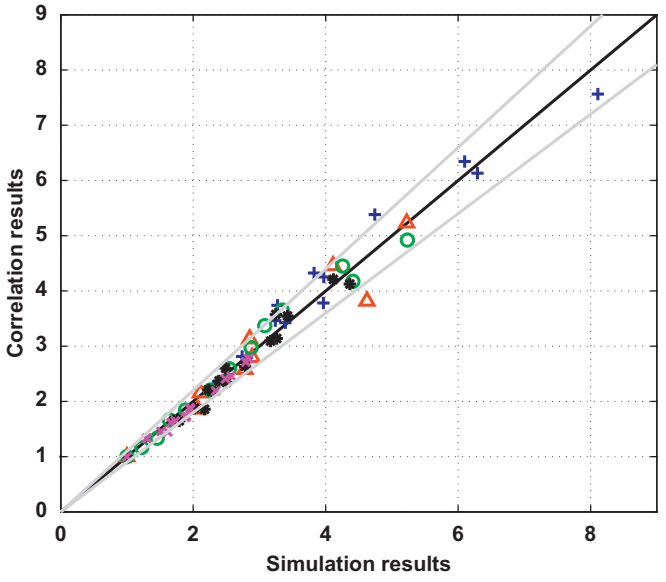

Fig. 6. A parity plot of the correlation results vs. the simulation results. Symbols are identical to Fig. 4. The gray lines indicate a deviation of 10% from the $y=x$ line.

was found to be 21%. These results are summarized in the parity plot shown in Fig. 6, comparing the correlation results to the simulation results (both in terms of $C_D/C_{D,\infty}(1-\alpha)$). Note that the limit of $\mathrm{Eo}\to 0$ yields an infinitely large drag coefficient, however, it can be expected that at such low Eötvös numbers, a Reynolds number dependency will be found rather than an Eötvös number dependency.

A comparison between the different correlations from literature and the new correlation derived in this work can now be made (see Fig. 7). We refer to Simonnet et al. (2007) for a concise overview of these correlations. Note that we have extrapolated the correlations to $\alpha=0.5$ if necessary. In Fig. 7, the drag on 4 mm air bubbles in water (Eo = 2.15) is compared. The correlation by Simonnet et al. (2007) is the only correlation that explicitly defines cooperative rise, for $\alpha>15\%$, while other correlations indicate that the normalized drag coefficient only increases as a

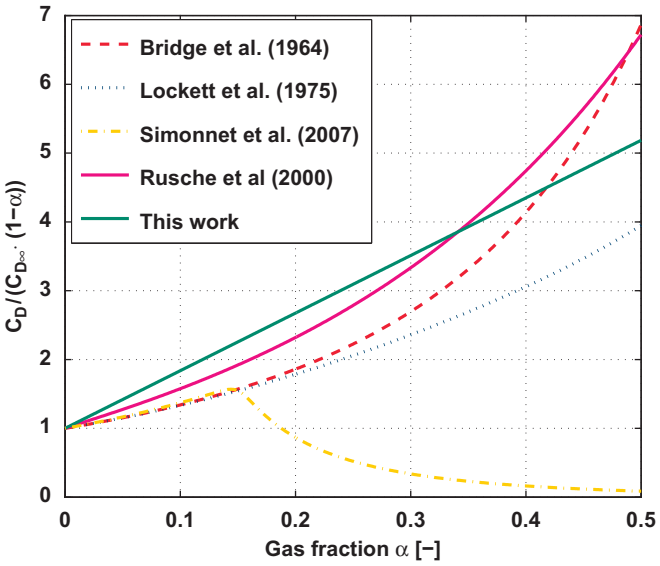

Fig. 7. A comparison between the different drag correlations.

function of the gas fraction as was also found in this work. The correlation presented in this work predicts the same order of magnitude for the drag correction as a function of the gas hold-up, however, it is the only correlation showing a linear relation with the gas hold-up, while other correlations show an exponential relation. The differences between the correlations may be caused by several factors, but the actual nature of this difference remains unknown at this point and further research is necessary to exclude one or more of these issues:

- The influence of contaminations has not been taken into account, while correlations derived from experiments could have strongly been influenced by this. In Dijkhuizen et al. (2010a) it was shown that DNS results of single rising bubbles perfectly match experiments with ultra-pure water from Veldhuis (2007), while experiments based on demineralised water yield a larger drag coefficient.
- The effect of coalescence and breakup, which occurs in experiments, makes it difficult to define a single bubble diameter (Eötvös number).
- The normalization, using the results of a single rising bubble, has been performed with different correlations or measurements.
- The results from the front-tracking model can only take local gas fractions into account, since the computational domain is small compared to the domain typically used in experiments. Apart from the correlation derived in this work, and the correlation from Simonnet et al. (2007), the literature correlations were explicitly defined for a global gas fraction, instead of a local gas fraction. This makes it also impossible to correct these correlations for the local gas hold-up, since the local gas hold-up is not known.

5.3. Morton dependency

The simulation results shown in Fig. 4 have been lumped into data series with identical Eötvös numbers, disregarding the fact that they may have different Morton numbers.

The cases that are lumped together are (see Table 2): 1 with 8 (Eo = 1.21), 4 with 6 (Eo = 2.58) and 5 with 7 (Eo = 4.83). It can be observed in Fig. 4, that for all cases, no different trends or otherwise distinctive features due to differences in the Morton numbers are visible. In the relatively small range of Morton numbers used in the simulations (between $\mathrm{Mo} = 2\times10^{-9}$ and 4×10^{-12}), the Morton number does not affect the drag coefficient.

6. Discussion

The developed drag closure was developed for mono-disperse bubble swarms, in the range of $1 < \mathrm{Eo} < 5$ and Morton numbers between 2×10^{-9} and 4×10^{-12}. When comparing this correlation to experimental results, it is important to note that, analoguous to Dijkhuizen et al. (2010a), the drag closure does not take effects of contaminations into account (i.e. pure liquid).

The results showed only hindered rise, while experimental results have shown an increase in the bubble rise velocity beyond a critical gas fraction (e.g. Simonnet et al., 2007). We attribute this to the lack of large-scale flow patterns in a full three-dimensional periodic domain, while flow patterns do emerge in a real-life column. A related issue, also considering the liquid flow field, is the sphere of influence of the liquid phase on a bubble rising in a swarm. Since the drag coefficient on a bubble has been determined using the bubble slip velocity, the definition of the liquid velocity should be defined in an exact manner. In this research, we have used the average liquid velocity throughout the computational domain; however, it may be argued that the range of influence around a bubble shrinks with increasing gas fraction. Additional studies are required to determine this range of influence, which is an important aspect in the implementation of the drag force in higher-level models.

The effect of inhomogeneities of the liquid flow field, resulting in additional lift and virtual mass forces, also needs additional research. In this work, local effects of lift and virtual mass forces are lumped into the newly derived correlation for the drag coefficient.

Because the rise velocity of the bubbles oscillates much more strongly than a single rising bubble, these velocity fluctuations might need to be taken into account in higher-level models. A study needs to be performed on the effect of these fluctuations (which may be implemented using an amplitude and most-occurring frequency) on the large-scale flow circulations.

7. Conclusions

A DNS front-tracking model was employed to develop a drag closure for bubbles rising in a mono-disperse swarm. We have selected eight different cases, with different Eötvös and Morton numbers, to investigate their influence, varying the gas hold-up up to 45%.

A remarkably simple correlation can describe the normalized drag coefficient for $1 \leq \mathrm{Eo} \leq 5$ very well, where no effect of the Morton number was found in the investigated range ($4\times10^{-12} \leq \mathrm{Mo} \leq 2\times10^{-9}$). This drag correlation has been implemented in the DBM code and was found to significantly improve the description of the hydrodynamics of bubble columns (Lau et al., this issue).

Nomenclature

Roman symbols

C_D	drag coefficient
d	diameter, m
$\overline{F}$	force, N
$\overline{g}$	gravity constant, m/s^2
m	mass, kg
p	pressure, Pa

$\overline{u}$	liquid, fluid velocity, m/s
$v,\overline{v}$	bubble velocity, m/s
V	volume, m^3
$\overline{w}$	fluid velocity, m/s

Greek symbols

α	gas fraction
ϕ	phase fraction in cell
μ	viscosity, Pa s*
ρ	density, kg/m^3
σ	surface tension coeff., Nm
τ	stress tensor

Abbreviations and subscripts

VM	virtual mass
b	bubble
D	drag
g	gas phase
G	gravity
l	liquid phase
L	lift
loc	local
glob	global
P	pressure
W	wall
∞	single rising bubble in an infinite quiescent liquid
Eo	Eötvös number
Mo	Morton number
Re	Reynolds number

Acknowledgments

This work is part of the research programme of the Foundation for Research on Matter (FOM), which is financially supported by the Netherlands Organisation for Scientific Research (NWO) and the Industrial partners of the IPP-FOM programme.

References

Acuña, C., Finch, J., 2010. Tracking velocity of multiple bubbles in a swarm. International Journal of Mineral Processing 94 (3–4), 147–158.

Bridge, A., Lapidus, L., Elgin, J., 1964. The mechanics of vertical gas–liquid fluidized system I: countercurrent flow. AIChE Journal 10 (6), 819–826.

Bunner, B., Tryggvason, G., 2002. Dynamics of homogeneous bubbly flows part 1. Rise velocity and microstructure of the bubbles. Journal of Fluid Mechanics 466, 17–52.

Clift, R., Grace, J., Weber, M., 1978. Bubbles, Drops and Particles. Academic Press, New York.

Darmana, D., Deen, N.G., Kuipers, J.A.M., Harteveld, W., Mudde, R., 2009. Numerical study of homogeneous bubbly flow: influence of the inlet conditions to the hydrodynamic behavior. International Journal of Multiphase Flow 35 (12), 1077–1099.

Deen, N.G., Van Sint Annaland, M., Kuipers, J.A.M., 2004. Multi-scale modeling of dispersed gas–liquid two-phase flow. Chemical Engineering Science 59 (8–9), 1853–1861 (Complex Systems and Multi-scale Methodology).

Dijkhuizen, W., 2008. Derivation of closures for bubbly flows using direct numerical simulations. Ph.D. Thesis, University of Twente.

Dijkhuizen, W., Roghair, I., Van Sint Annaland, M., Kuipers, J.A.M., 2008. Numerical derivation of the drag force coefficient in bubble swarms using a front tracking model. In: 6th International Conference on Computational Fluid Dynamics in the Oil and Gas, Metallurgical and Process Industries, pp. CFD08-070.

Dijkhuizen, W., Roghair, I., Van Sint Annaland, M., Kuipers, J.A.M., 2010a. DNS of gas bubbles behaviour using an improved 3d front tracking model-drag force on isolated bubbles and comparison with experiments. Chemical Engineering Science 65 (4), 1415–1426.

Dijkhuizen, W., Roghair, I., Van Sint Annaland, M., Kuipers, J.A.M., 2010b. DNS of gas bubbles behaviour using an improved 3d front tracking model–model development. Chemical Engineering Science 65 (4), 1427–1437.

Dijkhuizen, W., Van Den Hengel, E., Deen, N.G., Van Sint Annaland, M., Kuipers, J.A.M., 2005. Numerical investigation of closures for interface forces acting on single air–bubbles in water using volume of fluid and front tracking models. Chemical Engineering Science 60 (22), 6169–6175 7th International Conference on Gas–Liquid and Gas–Liquid–Solid Reactor Engineering.

Dijkhuizen, W., Van Sint Annaland, M., Kuipers, J.A.M., 2010c. Numerical and experimental investigation of the lift force on single bubbles. Chemical Engineering Science 65 (3), 1274–1287.

Lau, Y., Roghair, I., Deen, N.G., Van Sint Annaland, M., Kuipers, J.A.M. Numerical investigation of the drag closure for bubbles in bubble swarms. Chemical Engineering Science, this issue, doi:10.1016/j.ces.2011.01.053.

Lockett, M.J., Kirkpatrick, R.D., 1975. Ideal bubbly flow and actual flow in bubble columns. Transactions of the Institution of Chemical Engineers 53, 267–273.

Magnaudet, J., Eames, I., 2000. The motion of high-Reynolds-number bubbles in inhomogeneous flows. Annual Review of Fluid Mechanics, 659–708.

Martínez Mercado, J., Chehata Gómez, D., Van Gils, D., Sun, C., Lohse, D., 2010. On bubble clustering and energy spectra in pseudo-turbulence. Journal of Fluid Mechanics 650, 287–306.

Mei, R., Lawrence, C.J., Klausner, J.F., 1994. A note on the history force on a spherical bubble at finite Reynolds number. Physics of Fluids 6, 418–420.

Prosperetti, A., 2002. Navier–Stokes numerical algorithms for free-surface flow computations: an overview. Drop-surface Interactions. Springer Verlag, 2002, pp. 237–258.

Richardson, J., Zaki, W., 1954. Sedimentation and fluidisation: Part I. Transactions of the Institution of Chemical Engineers 32 (Supplement 1), 35–53.

Rusche, H., Issa, R., 2000. The effect of voidage on the drag force on particles, droplets and bubbles in dispersed two-phase flow. In: Japanese European Two-Phase Flow Meeting, Tsukuba, Japan.

Sankaranarayanan, K., Shan, X., Kevrekidis, I., Sundaresan, S., 2002. Analysis of drag and virtual mass forces in bubbly suspensions using an implicit formulation of the lattice Boltzmann method. Journal of Fluid Mechanics 452, 61–96.

Simonnet, M., Gentric, C., Olmos, E., Midoux, N., 2007. Experimental determination of the drag coefficient in a swarm of bubbles. Chemical Engineering Science 62 (3), 858–866.

Simonnet, M., Gentric, C., Olmos, E., Midoux, N., 2008. CFD simulation of the flow field in a bubble column reactor: importance of the drag force formulation to describe regime transitions. Chemical Engineering and Processing: Process Intensification 47 (9–10), 1726–1737.

Singh, R., Shyy, W., 2007. Three-dimensional adaptive cartesian grid method with conservative, interface restructuring and reconstruction. Journal of Computational Physics 224, 150–167.

Smolianski, A., Haario, H., Luukka, P., 2008. Numerical study of dynamics of single bubbles and bubble swarms. Applied Mathematical Modelling 32, 641–659.

Tomiyama, A., 1998. Struggle with computational bubble dynamics. In: Third International Conference on Multiphase Flow.

Tomiyama, A., Tamai, H., Zun, I., Hosokawa, S., 2002. Transverse migration of single bubbles in simple shear flows. Chemical Engineering Science 57, 1849–1858.

Unverdi, S., Tryggvason, G., 1992. A front-tracking method for viscous, incompressible, multi-fluid flows. Journal of Computational Physics 100 (1), 25–37.

van Sint Annaland, M., Deen, N.G., Kuipers, J.A.M., 2003. Multi-level modeling of dispersed gas–liquid two-phase flows. Heat and Mass Transfer. Springer, Berlin.

Van Sint Annaland, M., Dijkhuizen, W., Deen, N.G., Kuipers, J.A.M., 2006. Numerical simulation of behavior of gas bubbles using a 3-D front-tracking method. AIChE Journal 52, 99–110.

Veldhuis, C., 2007. Leonardos paradox: path and shape instabilities of particles and bubbles. Ph.D. Thesis, University of Twente, The Netherlands.